Title

Results from a Pre-Clinical Head Scanner for Proton CT

Authors

Johnson, RP
Bashkirov, V
Giacometti, V
et al.

Publication Date

2014

Peer reviewed

Results from a Pre-Clinical Head Scanner for Proton CT

R. P. Johnson, *Member, IEEE,* V. Bashkirov, V. Giacometti, R. F. Hurley, P. Piersimoni, T. E. Plautz, *Member IEEE*, H. F.-W. Sadrozinski, *Senior Member, IEEE,* R. Schulte, K. Schubert, *Senior Member, IEEE,* B. Schultze, N. Vence, M. Witt, A. Zatserklyaniy

***Abstract*– We report on the first beam test results with our pre-clinical (Phase-II) head scanner developed for proton computed tomography (pCT). After extensive preclinical testing, pCT will be employed in support of proton therapy treatment planning and pre-treatment verification in patients undergoing treatment with particle beam therapy. The Phase-II pCT system consists of two silicon-strip telescopes that track individual protons before and after the phantom or patient, and a novel multistage scintillation detector that measures a combination of the residual energy and range of the proton, from which we derive the water equivalent path length (WEPL) of the protons in the scanned object. The set of WEPL values and associated paths of protons passing through the object over a 360° angular scan is processed by an iterative, parallelizable reconstruction algorithm that runs on modern GP-GPU hardware. In order to assess the performance of the scanner, we have performed beam tests with 200 MeV protons from the synchrotron of the Loma Linda University Medical Center. The first objective was the calibration of the instrument, including tracker channel maps and alignment as well as the WEPL calibration. Then we performed the first CT scans on a series of phantoms. The very high sustained rate of data acquisition, exceeding one million protons per second, allowed a full 360° scan to be completed in less than 10 minutes, and reconstruction of a CATPHAN 404 phantom verified accurate reconstruction of the proton relative stopping power in a variety of materials.**

I. Introduction

Proton CT (pCT) is an evolving technology that promises to improve proton treatment planning by addressing the range uncertainty problem. It will generate a set of integrated relative stopping power (RSP) measurements that are used to reconstruct a 3-D map of RSP values to be input into a treatment planning system. Before proton CT can be implemented in clinical routine, it needs to be thoroughly evaluated. Our pCT Collaboration has built and successfully operated a Phase-II scanner [1] that measures *individually* more than a million protons per second, a hundred times faster than our previous Phase-I device [2]. At this rate a full scan can be completed in less than 10 minutes, a performance level that will allow us to complete a full pre-clinical performance evaluation of this new modality. Here we report on the hardware implementation and initial testing.

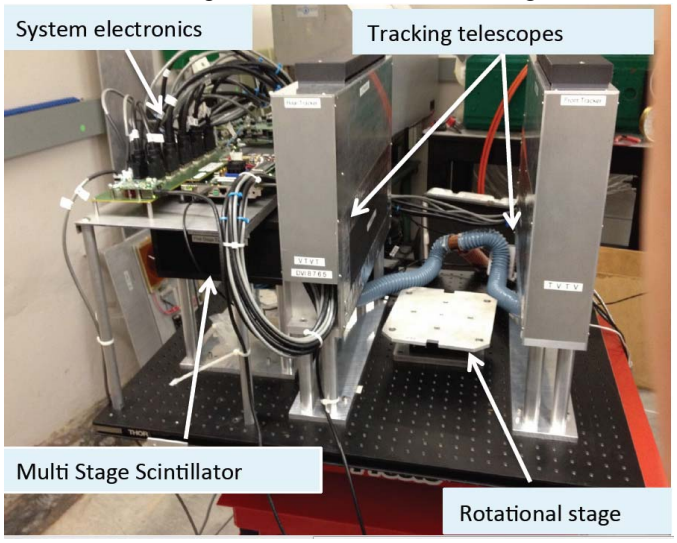

Figure 1. Photograph of the Phase-II pCT scanner in a proton beam line at the Loma Linda University Medical Center. The beam enters from the right.

Our Phase-II scanner (Figure 1) is based on two silicon-strip tracking-detector modules, an energy/range detector made from five scintillator stages read out by photomultiplier tubes, a rotating stage for the phantom, and a custom high-speed data acquisition system. The tracking system measures the proton entry and exit positions and directions from the phantom, while the energy/range detector measures the residual proton range. From the measurements we estimate the trajectory of the proton through the phantom and its water-equivalent path length. The stage rotates the phantom, typically in 2° or 4° steps with about 2 million or more protons per step, giving 90 or 180 views from which a 3-dimensional map of the phantom's RSP is reconstructed. We illuminate the full active

Manuscript received November 26, 2014. This work was supported in part by the National Institute of Biomedical Imaging and Bioengineering (NIBIB) and the NSF, award Number R01EB013118.

R. P. Johnson, T. Plautz , H. F.-W. Sadrozinski, and A. Zatserklyaniy are with the Santa Cruz Institute for Particle Physics and Physics Department, University of California at Santa Cruz, Santa Cruz, CA 95064 (e-mail: rjohnson@ucsc.edu, tiaplautz@gmail.com, hartmut@ucsc.edu, zatserkl@ucsc.edu).

V. Bashkirov, R. F. Hurley, P. Piersimoni, R. Schulte, and N. Vence are with the Division of Radiation Research, Loma Linda University, Loma Linda, CA 92354 (e-mail: vbashkirov@llu.edu, ford.hurley@gmail.com, pierluigi. piersimoni@gmail.com, rschulte@llu.edu, nvence@llu.edu)

K. Schubert and B. Schultze are with the School of Engineering and Computer Science, Baylor University, Waco, TX 76798 (e-mail: Keith_Schubert@baylor.edu, blake@r2labs.org)

V. Giacometti is with the Centre for Medical Radiation Physics, University of Wollongong, Wollongong, NSW, Australia (e-mail: valentina8giacometti @gmail.com).

M. Witt is with the Department of Computer Science and Engineering, California State University, San Bernardino, CA 92407 (e-mail: micah@r2labs.org).

area of the detector with protons by using a thin lead foil to scatter the beam just after it exits from the vacuum pipe.

Figure 2 is a display of the raw data from a single 200 MeV proton event from the synchrotron of the Loma Linda University Medical Center (LLUMC) [3]. The right-handed detector coordinate system is t, u, v, where the u coordinate points along the proton beam direction and the v coordinate points downward. Each of the two tracking detectors measures two coordinates in the v, u plane and two in the t, u plane, to give the incoming and outgoing vectors. The energy/range detector consists of five consecutive plastic scintillator stages read out by photomultiplier tubes (PMTs). The PMT signals are digitized at 65 MHz, and the figure shows the individual ADC samples for each stage. In normal running, however, the samples are summed in FPGAs located on the digitizer boards before sending the data to the event builder, to minimize the data volume and facilitate the required megahertz event rate.

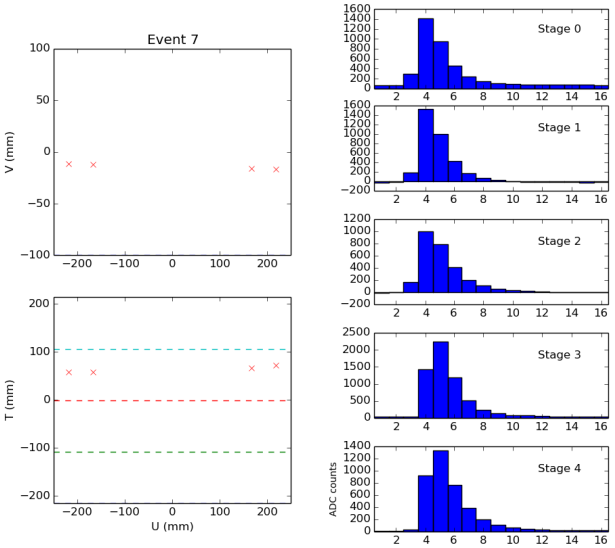

Figure 2. Display of the raw data of a single 200 MeV proton event. No phantom was present on the stage. On the left the crosses indicate all of the SSD strips with signal above threshold. The dashed lines in the t, u plot indicate the locations of gaps between SSDs. On the right are the raw outputs of the 65 MHz 14-bit pipelined ADCs that digitize the energy detector PMT waveforms. The proton stopped in Stage 4.

II. Tracking Detector

The tracking detector is based upon well-established silicon-strip detector (SSD) technology. SSDs are nearly ideal candidates for the tracking portion of a pCT system. The relatively high cost per square centimeter of the sensors (compared to plastic scintillators, for example) is more than offset by their high performance, reliability, stability, and ease of assembly. Furthermore, the sensor cost would be a minor portion of the overall cost of a clinical system. SSDs offer the following attractive characteristics, demonstrated in very large systems such as the Fermi-LAT Gamma-ray Space Telescope [4] and the CERN LHC tracking detectors [5][6]:

- near 100% efficiency for charged particle detection with practically zero noise occupancy,
- inherently fine spatial resolution (about 70 microns rms in this case),
- simple calibration that is stable over time periods of many years,
- and compact and easy assembly using standard mechanized industrial processes, with excellent mechanical stability.

Although there would be a small advantage, in terms of minimizing scattering material, to use double-sided detectors, our system uses single-sided detectors that were surplus items from fabrication of the Fermi-LAT silicon-strip tracker. The 0.4 mm SSD thickness was also optimized for the Fermi-LAT, but simulations showed only minor advantages to using thinner devices (because proton scattering in the object being imaged dominates).

A very important parameter is the size of the gap between individual sensors. We minimized that by re-sawing the SSD edges very close to the guard ring, such that the distance between active regions of adjacent sensors is only about 0.6 mm. That caused a dramatic increase in leakage current, but none of the excess current flowed to the readout amplifiers, and the SSD noise performance was not impacted. With more time and resources we could have minimized the leakage current by cleanly cleaving the silicon and then passivating the edges [7].

The front-end of the data acquisition for the tracking detector is based on a custom integrated circuit (ASIC) that is described elsewhere [8]. FPGAs on each detector board combine and format the data from groups of 12 ASICs and then send the data over dual-link DVI-D cables to the event builder. Figure 3 shows a photograph of one of the detector boards.

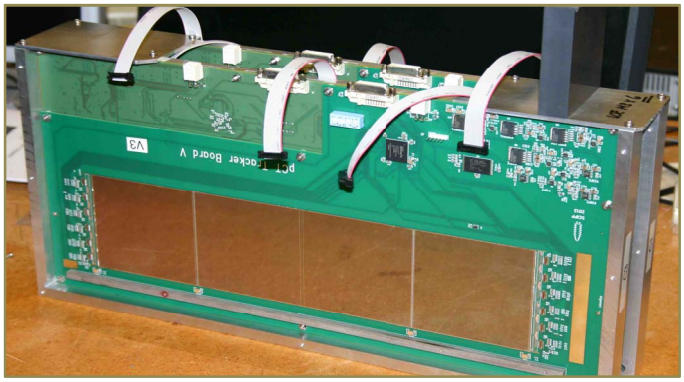

Figure 3. One of the two tracking modules, with two v layers and two t layers, removed from its enclosure. A v tracking layer is visible, on which the silicon strips run horizontally. Strips on pairs of SSDs are wire bonded together and read out by six ASICs on each end of this board. Each t layer has strips running vertically, and each SSD is read out by six ASICs, for a total of 24 per t board. The loose cables visible here are for programming the six Xilinx Spartan-6 FPGAs, one per V board and two per t board.

High efficiency with low noise is an essential requirement for the tracking detector. There is almost no redundancy in the tracking—all eight coordinate measurements ("hits") are needed for each proton. Some protons do pass through the small gaps between sensors (which are staggered from one layer to the next), but in most cases those events can be

recovered as follows [9]. In t layers the gaps are parallel to the strips. If the strips are 100% efficient, then a missing hit indicates that the proton passed through the gap, which localizes it in t almost as accurately as a hit strip does. A missing hit in a v layer of the front tracking module can be recovered by using our knowledge of the beam origin at the exit from the vacuum pipe, which is accurately located from extrapolations of millions of proton tracks. From analysis of 200 MeV proton data with no phantom we have measured the SSD efficiency within the active area to be 99.9%. The gaps lower the overall efficiency of a layer by about 0.5%, but most of the missing hits can be recovered as explained above.

III. Multi-Stage Energy/Range Detector

Our Phase-I scanner used doped CsI crystals to measure the residual proton energy. While such crystals yield excellent energy resolution, they are too slow for the high rates needed in a clinical system. In the Phase-II system, by dividing the energy detector into five stages, we greatly reduced the requirement on energy resolution, allowing effective use of fast plastic scintillators. Stages through which the proton passes directly measure contributions to total range, so the last segment, in which the proton stops, need measure only a small residual range, with only a relaxed precision requirement.

We developed a custom board to digitize the PMT signals, with each board handling up to three channels. Each 14-bit ADC can operate at rates up to 65 MHz, yielding digitized waveforms as illustrated in Figure 2. An FPGA on each board buffers the data and, upon receipt of a trigger, reduces the data by summing six samples around the peak of the pulse (one before and four after). A separate amplifier-discriminator chain in each channel provides asynchronous signals for the trigger logic, although in normal operation we trigger the readout from just the first stage, as it is the only one guaranteed to have a signal in every event.

When we look at just the signals in the first stage from 200 MeV protons passing through a 2 cm square in the center of the detector (with no phantom in place), we find a Gaussian distribution with $\sigma = 3.0\%$. Since Geant4 simulations [10] predict $\sigma = 2.8\%$ just from variations in the energy deposition, we estimate that the detector resolution is around 1%, more than adequate for this application.

The detector does show a small, stable dependence on T and V that must be measured from the data and corrected. After that is done, then we calibrate the measurement of Water Equivalent Path Length (WEPL) by taking and analyzing proton data with a large number of different known thicknesses of polystyrene placed between the two tracking detectors [11]. To facilitate this process we developed a novel phantom composed of five separable pieces of polystyrene [12]. The first piece is machined into six sets of stairs, while the other four are rectangular blocks (see Figure 4). The tracking system is used to calculate which step in the stairs each proton passed through. By taking only six ten-second runs, one with no phantom, one with just the stairs, and four with one to four rectangular blocks in place as well, we accumulate a dataset of many millions of protons with 45 different thickness of polystyrene in 6.35 mm steps. We have verified that this procedure yields a WEPL resolution that is approximately 3 mm for all values of WEPL, only slightly higher than the predicted lower limit of 2.75 mm that arises from range straggling of 200 MeV protons.

Since the energy/range detector has no lateral segmentation, it can effectively analyze only a single proton per accelerator RF period (about 118 ns for 200 MeV protons from the LLUMC synchrotron). Therefore, we must reject events with two or more proton tracks detected, which effectively limits the practical event rate to not much more than a megahertz. The accelerator has to be operated at a very low intensity of about one proton per nine RF periods on average.

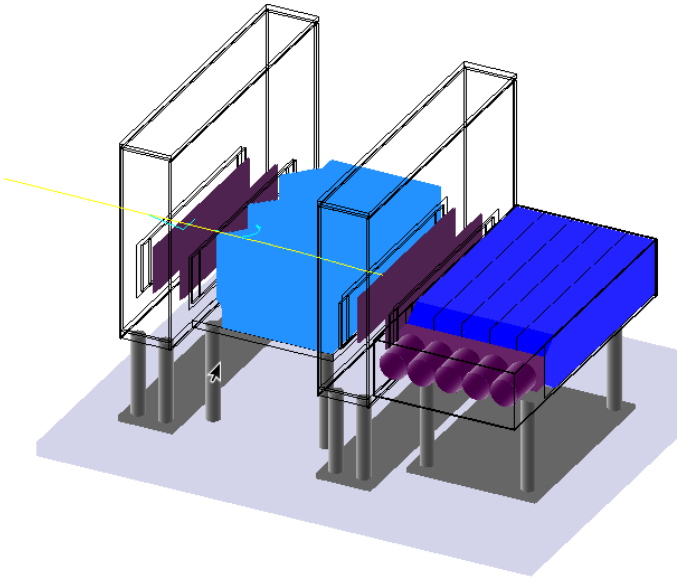

Figure 4. Graphical depiction (from our Geant4 model) of the Phase-II scanner with the WEPL calibration phantom installed. The incoming line represents the trajectory of a simulated proton.

IV. Data Acquisition

The data acquisition system was designed to move the raw data from at least a million events to the computer per second. It does so in several stages. The raw digitized data are delayed in FIFOs at the front end (in the ASICs for the tracking boards and in the FPGAs for the energy detector boards) until a trigger is received. In a tracking board the data, in the form of a list of clusters of strips above threshold, flow in parallel from 12 ASICs to an FPGA, at a rate of 100 Mbit/s for each link. The ASICs buffer up to four events to smooth out random fluctuations in the proton arrival times. The FPGA buffers the incoming data and builds a packet from the contributions of the 12 ASICs—in a typical event only a single ASIC contributes a cluster. Similarly, the FPGA on each energy detector board buffers the event data and in parallel reduces the 14-bit ADC values down to a summed pulse height per channel.

The 14 front-end FPGAs then send their data packets at 100 Mbit/s each over dual-link DIV-D cables into the buffers of the event builder, a Xilinx Virtex-6 FPGA. Once all data from a

given trigger are present in the event builder, they are packaged together and sent to the data acquisition computer over a 100 MByte/s Ethernet link.

The data integrity is monitored via parity bits in the ASIC-to-FPGA transmission and an 11-bit CRC in the transmissions between FPGAs. Also, the data are given trigger tags at the front end, and the system checks that the tags match throughout the event building, to detect possible mixing between events. The commands transmitted between FPGAs and from FPGA to ASIC are also monitored by parity bits. In our most recent beam test, 2.5 billion events with a total of 1.8×10^{11} bytes were acquired with zero errors of any kind detected.

Figure 5 shows the rate performance during a single short run. The proton rate from the accelerator is nonuniform during a spill, but the system gracefully inhibits the trigger when all buffers are full and keeps data flowing at the maximum allowed rate. In this case the sustained event rate of just over a megahertz was limited by the program running in the computer. The data acquisition system itself can sustain a rate of nearly 1.3 MHz, as indicated here by the performance at the beginning of the spill, before the computer backed up the flow.

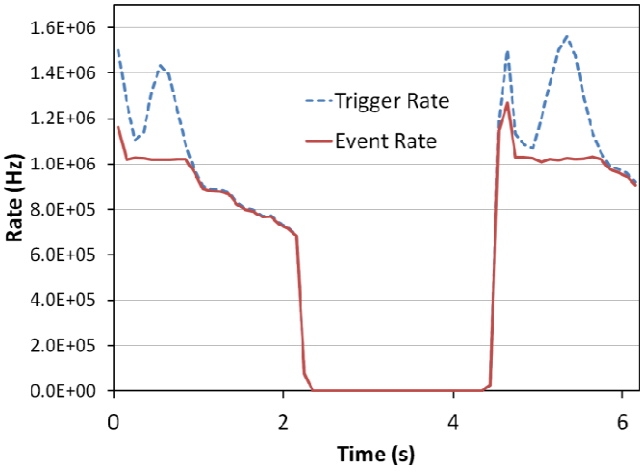

Figure 5. Example run with 200 MeV protons, showing two spills from the synchrotron. Up to about 1 MHz, nearly 100% of the triggers are accepted.

V. Image Reconstruction

Figure 6 shows an example reconstructed image of a CATPHAN 404 sensitometry phantom. The reconstruction employed a filtered back-projection (FBP) followed by an iterated algebraic reconstruction (TVS with DROP [13]) that makes use of the tracking information of individual protons to define a most-likely-path (MLP) through the phantom for each [14]. The relative stopping power (RSP) of a variety of materials is accurately measured, as demonstrated in Figure 7.

Work is in progress within our collaboration to employ space-carving algorithms to define the reconstruction volume and eliminate the FBP. Progress has also been made on parallelized reconstruction algorithms that run on an array of GPUs. Full image reconstructions have been completed in less than eight minutes, similar to the beam time required to acquire the data.

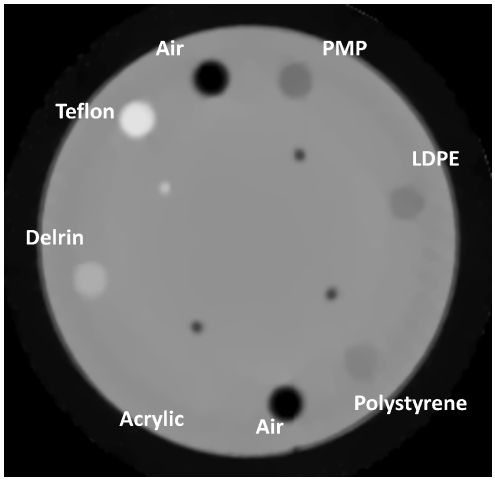

Figure 6. The first CT image reconstructed with data from the completed Phase-II scanner: a CATPHAN 404 phantom.

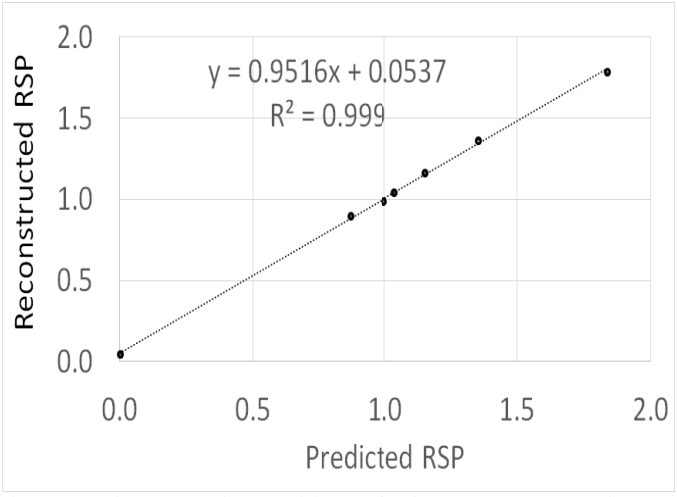

Figure 7. The measured RSP of inserts in the CATPHAN 404 phantom compared with the predicted values.

VI. Conclusion

The Phase-II head scanner hardware and data acquisition system have been completed and are operating reliably at the design data rate. Preliminary image results are encouraging. The system is now ready to support testing of reconstruction algorithms as well as a thorough evaluation of proton computed tomography in terms of image resolution [15], RSP measurement, and dose in a variety of phantoms, including comparisons with detailed Monte Carlo simulations [16].

Acknowledgment

The authors thank the Xilinx Corporation for donating the Virtex-6 FPGA evaluation boards and associated programming hardware and software. They also acknowledge crucial support from the technical staff at UCSC and LLU, including the accelerator operating staff at LLUMC. The content of this paper is solely the responsibility of the authors and does not necessarily represent the official views of NIBIB and NIH.

REFERENCES

[1] H.F.-W. Sadrozinski, *et al.,* "Development of a Head Scanner for Proton CT," Nucl. Instr. Meth. A, vol. 699, pp. 205–210, 2013.

[2] H. F.-W. Sadrozinski, *et al.,* "Detector Development for Proton Computed Tomography (pCT)," 2011 IEEE Nuclear Science Symposium Conf. Record, pp. 4457–4461, Oct. 2011.

[3] G. Coutrakon, *et al.,* "A performance study of the Loma Linda proton medical accelerator," *Med. Phys.*, vol. 21, no. 11, pp. 1691-1701, 1994.

[4] W. B. Atwood *et al.,* "The Large Area Telescope on the Fermi Gamma-ray Space Telescope mission," Ap. J., vol. 697, p. 1071, 2009.

[5] ATLAS Collaboration, "The ATLAS Experiment at the CERN Large Hadron Collider," JINST, vol. 3, S08003, 2008.

[6] CMS Collaboration, "The CMS Experiment at the CERN Large Hadron Collider," JINST, vol. 3, S08004, 2008.

[7] M. Christophersen *et al.,* "Alumina and Silicon Oxide/Nitride Sidewall Passivation for p- and n-type Sensors," Nucl. Instr. Meth. A, vol. 699, pp. 14–17, 2013.

[8] R. P. Johnson *et al,* "Tracker Readout ASIC for Proton Computed Tomography Data Acquisition," IEEE Trans. Nucl. Sci., vol. 60, pp. 3262-3269, 2013.

[9] A. Zatserklyaniy, *et al.,* "Track Reconstruction with the Silicon Strip Tracker of the Proton CT Phase-2 Scanner," presentation J03-6 of this conference.

[10] S. Agostinelli *et al.,* "Geant4–A Simulation Toolkit," Nucl. Instr. Meth. A, vol. 506, p. 250, 2003.

[11] R. F. Hurley, *et al.,* "Water-Equivalent Path Length Calibration of a Prototype Proton CT Scanner," Med. Phys., vol. 39, no. 5, pp. 2438-2446, 2012.

[12] V. A. Bashkirov, *et al.,* "A Novel Phantom and Method for Calibration of the Phase II Proton CT Scanner," presentation M19-52 at this conference.

[13] S. N. Penfold, *et al.,* "Total Variation Superiorization Schemes in Proton Computed Tomography Image Reconstruction," Med. Phys., vol. 37, no. 11, pp. 5887-5895, 2010.

[14] D. C. Williams, "The most likely path of an energetic charged particle through a uniform medium". Phys. Med. Biol. 49 (2004) 2899–2911.

[15] T. Plautz, *et al.,* "Spatial Resolution Studies and Measurement of the Modulation Transfer Function for a Prototype Proton CT Scanner," presentation M19-53 at this conference.

[16] V. Giacometti, *et al.,* "Geant4 Simulation Platform for the Phase-2 Proton CT Scanner," presentation M19-67 at this conference.